The Extracellular Domains of ErbB3 Retain High Ligand Binding Affinity at Endosome pH and in the Locked Conformation†

Kian Kani,‡ Euisun Park,‡ and Ralf Landgraf*,‡,§,||

Department of Medicine, Hematology-Oncology, and Department of Biological Chemistry, and Molecular Biology Institute, University of California, Los Angeles, California 90095

Received July 29, 2005; Revised Manuscript Received September 23, 2005

ABSTRACT: The extracellular, ligand binding regions of ErbB receptors consist of four domains that can assume at least two alternative conformations, extended and locked. The locked conformation, observed in several crystal structures, is held together by a noncovalent intramolecular tether and is incompatible with current models for receptor dimerization and ligand activation. Based on structures of ligand−receptor complexes in the extended conformation, the high affinity ligand binding pocket between domains I and III is disrupted in the locked conformation. Therefore the biological role of the locked conformation is not clear. To address the impact of the locked conformation on ligand binding, we compared extracellular domains of wild-type ErbB3, mutant domains in a constitutively locked or extended conformation and partial extracellular domain constructs. We found that the constitutively locked receptor domains and truncated constructs carrying only domains I−II or III−IV strongly bind ligand, albeit with reduced affinity compared to wild-type receptor. This suggests that the locked conformation cannot be discounted for ligand binding. The significant binding by both partial interfaces in domains I and III also suggests that "partial bivalency" may be the reason for the low nanomolar and high picomolar binding observed for ErbB3 in the respective "low" and high affinity states. In contrast to EGFR (ErbB1), ErbB3 retains high ligand binding affinity at an endosome-comparable pH in both the extended and locked conformations. Ligand affinity for the locked conformation even improves at low pH. For ErbB3, the contribution of domain I to ligand binding is strong and increases at low pH while its contribution is thought to be minimal for EGFR, regardless of pH. This shift in domain contribution and pH dependency provides a mechanistic explanation for some of the divergent properties of EGFR and ErbB3.

Signaling by ErbB receptors involves the ligand-induced activation of dimeric complexes of receptors. In the case of ErbB3, binding of the EGF-like ligand heregulin (neuregulin) results primarily in the activation of dimers of ErbB2 and ErbB3 and leads to tyrosine phosphorylation of the cytoplasmic portions of both receptors. Of the various receptor combinations that can form among the four human ErbB receptors, the signaling through the ErbB2−ErbB3 receptor combination represents the most potent promitotic signal (*1*), utilizing the strong ligand binding properties of the kinase deficient ErbB3 and the potent kinase activity of ErbB2, which by itself is deficient in ligand binding (*2*, *3*). Overexpression and constitutive activation of ErbB2 can be found in several types of cancers (*4*−*8*), and the proliferative effects of overexpression are further enhanced by elevated levels of ErbB3.

The mechanism by which the activity of ErbB receptors is controlled has received renewed attention, and much of the current knowledge has been derived from EGFR, which has traditionally served as a model for most aspects of ErbB signaling. Activation was long thought to be primarily controlled by ligand-induced dimerization. However, while dimerization is essential for tyrosine phosphorylation, several lines of evidence suggest that the receptors can dimerize in the absence of ligand (*9*−*13*). Furthermore, the kinase domain of EGFR has long been known to be unique in that its activation loop does not require phosphorylation of a critically conserved tyrosine (*14*), and its crystal structure confirmed that the activation loop can indeed adopt the active conformation without the need for phosphorylation (*15*). This suggests that the key question for ErbB signaling may not be how the receptors can be activated, but how their constitutive activity can be suppressed in the absence of ligand. In the case of EGFR, signaling has also been shown not to be limited to the cell surface. Receptor activation and signaling to downstream components can occur from endocytosed receptors (*16*, *17*), and experiments using delayed activation have demonstrated that signaling initiated from endosomes is sufficient to activate key downstream pathways (*18*).

Crystal structures of the extracellular domains (ECD) of the homologous EGFR in the presence of ligand have provided insight into the ligand binding and dimerization interface of the activated receptor (*19*, *20*). The ECD of ErbB receptors consists of four domains (Figure 1) with high

† This work was supported by NIH Grant R01 CA098881 (R.L.).

* Address correspondence to this author. Mailing address: Department of Medicine, Hematology-Oncology, Box 951678, Los Angeles, California 90095-1678. Tel: 310 206-7239. Fax: 310 825-2493. E-mail: rlandgraf@mednet.ucla.edu.

‡ Department of Biological Chemistry.

§ Department of Medicine, Hematology-Oncology.

|| Molecular Biology Institute.

10.1021/bi0515220 CCC: $30.25
Published on Web 11/03/2005

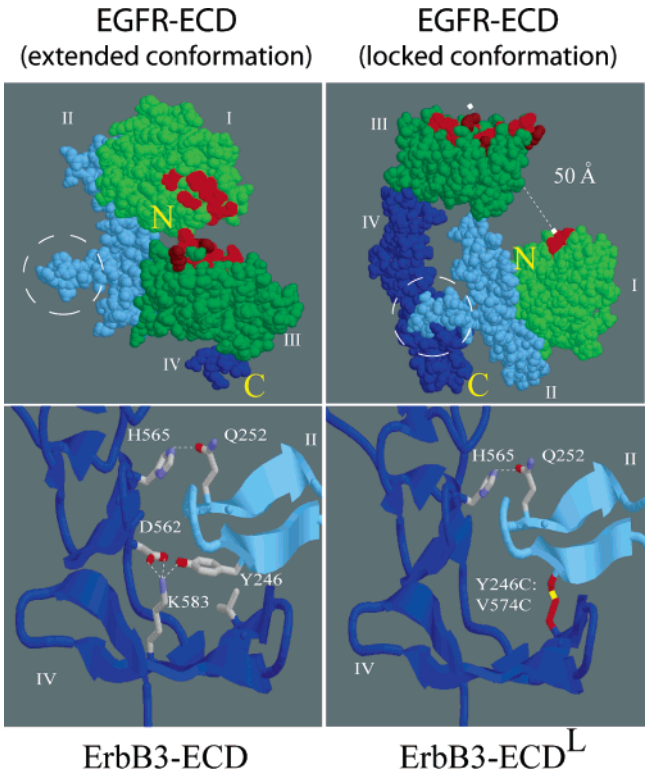

FIGURE 1: Relative orientation of the ligand binding sites in domains I and III of EGFR (top), and nature of the locking tether in wild-type and constitutively locked ErbB3 (bottom). Top: The space filling diagram of the ECD of EGFR in the extended conformation (*20*) (left) and the locked conformation (*32*) (right), demonstrating the rotation and spatial separation of the ligand binding interfaces in domains I and III as a result of the transition from the extended to the locked form. Domain I (amino acids 1−190) is colored light green; domain II (amino acids 191−309) is colored light blue; domain III (amino acids 310−500) is colored dark green; domain IV (amino acids 501−622) is colored dark blue (truncated in the structure of the extended conformation). The residues that contact the ligand in the cocrystal structure are colored red, and those that are histidines are colored dark red. The dashed line represents the distance between L69 and Q384 at the center of each interface. The white circle marks the position of the loop in domain I positioned to engage another EGF receptor (left) or domain IV in the intramolecular lock (right). Bottom: Interactions that stabilize the locking tether in wild-type ErbB3 (left) and location of the additional disulfide bridge in the constitutively locked ECD^{L} (right). Domain II is colored in light blue and domain IV in dark blue. Dashed lines represent hydrogen bonds between H565 and Q252, Y246 and K583, and D562 and K583. The additional disulfide bridge between Y246C and V574C is colored in yellow.

homology between domains I and III (light and dark green in Figure 1) as well as II and IV (light and dark blue in Figure 1). Biochemical and structural evidence support a model of a ligand binding pocket formed between domains I and III (critical residues for the interaction of EGF with EGFR are outlined red in Figure 1). Within this common structural framework, the exact contribution by domain I versus III to ligand binding may differ for different receptors in this family.

The crystal structure of the dimer of the extracellular domains of EGFR with bound ligand demonstrated that the ligand is placed on the outside of the dimer and does not mediate dimerization directly. Instead dimerization involves a critical loop in domain II of each receptor (marked by a white circle in Figure 1), which interacts with domain II of the second receptor in a symmetrical fashion. Mutational analysis of this loop has confirmed its role in ligand-induced activation showing impaired activation and faster ligand dissociation from the mutated receptor (*13*, *21*). A corresponding loop in the homologous domain IV is believed to be part of the dimerization interface as well, facilitating symmetrical interactions of domain IV on both receptors. However, domain IV was either absent or not resolved in the crystal structure and hence its specific contribution to interactions in receptor dimers is less clear. The crystal structure of the ligand-free extracellular domains of ErbB2 has revealed a monomeric receptor in an extended conformation, largely corresponding to the overall arrangement of domains in the structure of dimeric EGFR. This extended conformation is believed to represent an ErbB2 receptor predisposed to undergo dimerization (*22*−*24*).

In contrast to ErbB2 and ligand bound EGFR, the crystal structure of the extracellular domains of ErbB3, solved in the absence of its ligand heregulin, revealed a locked conformation. In this locked or "tethered" conformation, the two putative dimerization loops in domains II and IV instead interact within the same receptor molecule (*25*). An equivalent locked conformation has since been observed in a crystal structure of the extracellular domains of EGFR (*26*) (Figure 1, top). In contrast to the structure solved for ErbB3 at pH 9.0, crystals for this structure were derived at pH 5.0 and show ligand bound to domain I of EGFR.

Ligand binding to domain I has been observed previously for the homologous ErbB3 receptor (*27*), and biochemical and structural evidence for EGFR supports a mode of binding with contacts to domains I and III (*19*, *20*, *28*, *29*). However, the main stabilizing interactions are thought to come almost exclusively from domain III (*30*, *31*). The binding to domain I of EGFR at crystallization conditions and low pH is thought to reflect the low affinity binding to this site (K_D > 50 μM (*26*)) under conditions in which the protonation of critical histidines in the interface of domain III (dark red in CPK representation of EGFR in Figure 1) renders this interface nonfunctional (*19*, *26*).

The formation of the intramolecular tether or lock, observed for ErbB3 and EGFR, initially provided an attractive model for the control of ErbB receptors. In this model, the lock is a critical feature needed to suppress constitutive receptor dimerization and activation (*26*, *32*, *33*). However, the formation of the intramolecular lock does not appear to be the solution to the question of how to control the activity of ErbB receptors with intrinsically active kinase domains. Mutations in critical residues of the intramolecular lock in EGFR have revealed only a minor role for the locked conformation in the suppression of constitutive receptor activation. For EGFR, lock deficient mutants show an increase in high affinity binding sites and a decreased rate of EGF dissociation, but no significant increase in constitutive activation or differences in EGF induced signaling (*13*, *21*).

For ErbB3, insight into the contribution of the locked and unlocked states to receptor activation and association states can be drawn from chimera of ErbB3 and ErbB2 (*34*). Such chimera add the transmembrane span and catalytic activity of ErbB2 cytoplasmic portions to the otherwise catalytically inactive ErbB3. This fusion provides cytoplasmic tyrosine phosphorylation as an additional readout for the changes imposed by the ligand on the interactions of the extracellular

domains of ErbB3. The additional stabilization of dimers provided by the transmembrane span of ErbB2 is critical for function as comparable chimera with transmembrane spans of ErbB3 fail to respond to ligand (*35*). Compared to chimera with wild-type ECDs, the ligand independent activation of constitutively extended chimeras is only marginally elevated. This suggests an additional mechanism for the suppression of constitutive activity, possibly involving alternative modes of packing for the transmembrane spans of ErbB receptors (*36*, *37*), but leaves the function of the locked form of the receptor unclear.

In an alternative approach to address the function of the locked conformation in a cellular context, the stabilization of the locked conformation has been attempted by engineering an additional disulfide bond. However, the analysis of this double mutant has been complicated by the fact that the extracellular domains of the wild-type receptor already contains fifty disulfide-bridged cysteines and the correct folding or formation of such constructs could not be verified in a cellular setting (*13*). A small portion of receptors (<10%) exhibited binding in the low nanomolar range but failed to transition to a high affinity binding mode characteristic for activated EGFR. However, other studies have concluded that the locked or tethered conformation is unlikely to represent the low affinity binding mode of EGFR (*21*). In the absence of data that demonstrate the correct formation of the engineered disulfide bridges, the available data on ligand binding of receptors in the locked conformation remain inconclusive. Therefore other strategies to assess the importance of the locked species were needed.

A key question for the biological relevance of the locked conformation for ErbB receptors is whether the ligand receptor interaction between domain I and EGF, observed in the crystal structure of the locked conformation of EGFR, is relevant for other receptors such as ErbB3. Truncated constructs of ErbB3, consisting of domains I and II, show relatively strong binding to ligand (67 nM compared to 2 nM for full-length ECDs) (*27*). This would suggest that the interaction of ErbB3 with its ligand heregulin differs in several key aspects from EGFR, namely, in the relative contribution of domains to ligand binding. For EGFR, ligand binding depends almost exclusively on domain III interactions, and EGFR also differs from ErbB3 in the overall strength of receptor ligand interactions. While binding constants of EGF to the ECD of EGFR are in the range of 500 nM (*30*), the binding of heregulin to purified ECDs of ErbB3 determined by different methods has been placed for the majority of measurements at around 1−10 nM (Table 1). This relatively strong binding is considered to represent the "low" affinity binding mode for the ErbB3 receptor, and binding to ErbB3/ErbB2 heterodimers as well as tyrosine phosphorylation response occurs in the high picomolar range (*38*−*40*).

However, it is not clear if ligand binding to ErbB3 can occur in the locked conformation, or if the conformation of the locked species precludes all binding of the ligand at physiologically relevant concentrations. A failure of the locked ECD to bind ligand with appreciable affinity would have mechanistic implications and would suggest that the ligand can only bind to ECDs that have stochastically assumed the extended conformation. Alternatively, if the ligand is capable of binding with a competitive affinity to either domain I or III under conditions in which the joint binding pocket is disrupted, this would allow a "capture" of the ligand in a reduced affinity mode, which is more likely to transition to a higher affinity binding mode involving interactions with both domains I and III. As a consequence, this subsequent bivalent and stronger interaction with domains I and III is likely to stabilize the extended and dimerization-competent conformation.

Table 1: ErbB3-ECD in the Locked Conformation Binds Heregulin with Comparable Affinity to the Domains I and III[a]

ErbB3 construct	K_D (pH 7.4)	published [method] (ref)
ECD	5 ± 2 nM	5.4 nM (hrgβ1), 550 nM (hrgα) [PE] (*51*)
		8.2 nM [PE] (*52*)
		1.3 nM [SPR] (*3*)
		2.3 nM [SPR] (*27*)
		4.7 nM [PE] (*53*)
		3.0 nM [PE*] (*53*)
		26 nM [LS+SE] (*54*)
		0.9 nM [IC] (*55*)
		2 nM [COS] (*39*)
		11 nM [COS] (*56*)
		249 nM satSPR (*57*)
ECD^{E}	1 ± 1 nM	na
ECD^{L}	52 ± 13 nM	na
ECD^{I-II}	49 ± 3 nM	67 nM [SPR] (*27*)
ECD^{III-IV}	9−90 nM[b]	na

[a] Binding constants at pH 7.4 were derived arithmetically from estimates of dissociation on- and off-rates, obtained in individual runs. Published K_Ds are listed where available, and abbreviations represent the following methods: [PE] = plate ELISA with immobilized receptor or fusion and radiolabeled hrg; [PE*] = same as PE but naturally occurring soluble and truncated ECD, missing the second half of domain 4; [LS+SE] = light scattering and sedimentation equilibrium; [IC] = insect cells carrying only recombinant ErbB3; [COS] = COS cells carrying only recombinant ErbB3; [satSPR] = saturation binding study by SPR. [b] ECD^{III-IV} is the only construct for which large deviations for its K_D were obtained when measured at different ECD concentrations (see Discussion).

In order to evaluate the ligand binding properties of the locked species of ErbB3, we have created a constitutively locked species of the ECD of ErbB3 that is secreted from S2 cells and can readily be evaluated for stability, folding, correct formation of the engineered disulfide bridge, and ligand binding. Our analysis of the locked ECD shows relatively high affinity for heregulin, comparable to the isolated binding sites in domains I and III. The latter were evaluated in constructs carrying domains I and II (ECD^{I-II})[1] or III and IV (ECD^{III-IV}) for solubility reasons. Surprisingly, and in contrast to EGFR, binding of ligand by the locked species of ErbB3-ECD improves with low pH and achieves the highest binding affinity at pH 5.5. This is consistent with the observation that the full-length ECD, in contrast to EGFR, also retains ligand binding at lower pH. This increase in affinity of the locked conformation at lower pH is best mirrored by the binding behavior of ECD^{I-II} but not ECD^{III-IV}, consistent with our earlier observation that for ErbB3, but not EGFR, domain I is a key contributor to ligand

[1] Abbreviations: trx-hrg, fusion protein of thioredoxin and EGF-like domain of heregulin; SPR, surface plasmon resonance; PBS, phosphate buffered saline; ECD, extracellular domain; ECD^{I-II} and ECD^{III-IV}, truncated ECD consisting of domains I−II or III−IV, respectively; ECD^{E}, constitutively extended ECD; ECD^{L}, constitutively locked ECD; hrg, EGF-like domain of heregulin; trx-hrg, fusion protein of thioredoxin and the EGF-like domain of heregulin.

binding. This distinct ability of ErbB3 to retain ligand binding at low pH may also have consequences on the ability of the receptors to retain the ligand in sorting endosomes, and the locked conformation may likewise play a more significant role in the endosome compartment than the cell surface.

MATERIALS AND METHODS

Plasmids and Protein Purification. ErbB3-ECD cDNA was cloned into the pMT/BiP/V5-His expression vector (Invitrogen, Carlsbad, CA) as previously described (*41*). The Y246C:V574C, V245C:A577C mutations and truncated ECD^{I-II} and ECD^{III-IV} constructs were generated using two-step PCR and subsequently confirmed by sequencing. The ECD^{I-II} construct includes residues 1−309, and the ECD^{III-IV} construct includes residues 310−610. *Drosophila* S2 cells were cotransfected with the desired constructs and the pCoHYGRO vector (Invitrogen) using Effectene reagent (Invitrogen). Stable cell lines were obtained after three weeks of selection with 300 μg/mL hygromycin B (Invitrogen). Cells were grown in serum-free media (Hyclone, Logan, UT) and induced with 500 μM $CuSO_4$. The ECD constructs were purified by Ni-NTA column chromatography as previously described (*41*), dialyzed in phosphate buffered saline (PBS, 150 mM NaCl, 2.5 mM KCl, 81 mM Na_2HPO_4, 14.7 mM KH_2PO_4), and judged >95% pure by SDS−PAGE. Human heregulin-β 1 was generated as a fusion protein to the C-terminus of thioredoxin (trx-hrg) in the pET-32a vector (Novagen, Madison, WI) and expressed and purified from *Escherichia coli* BL21 (DE3) as previously described (*41*). The trx-hrg fusion protein has binding properties to the ErbB3-ECD that are equivalent to the EGF-like domain of hrg and carries an S-tag and hexa-histidine-tag, facilitating purification and detection.

Circular Dichroism Spectroscopy. The CD spectrum of wild-type ErbB3-ECD (2.5 μM) and ECD^L (1.75 μM) in PBS was measured on a JASCO J-715 spectropolarimeter (Easton, MD). Each run was conducted at 20 °C with a sensitivity of 20 mdeg at a resolution of 0.5 nm. The spectra are the result of four consecutive and cumulative runs that spanned from 198 to 260 nm. Spectra of the sample buffer were used for background subtraction. The spectra of both species were normalized for concentration and smoothed using adjacent averaging.

Analytical Ultracentrifugation. Sedimentation velocity analysis on ErbB3-ECD^L (0.30 mg/mL in PBS) was performed in a Beckman Optima XL-A analytical ultracentrifuge at 55,000 rpm and 20 °C using absorption optics at 280 nm and a 12 mm path length double sector cell. The sedimentation coefficient distribution was determined from a $g(s)$ plot using the Beckman Origin-based software (Version 3.01). The peak sedimentation coefficient was corrected for density and viscosity to an $S_{20,w}$ value using a value for the partial specific volume at 20 °C of 0.710, calculated from the amino acid composition (*42*) and corrected to 20 °C (*43*) and carbohydrate content (*44*). Sedimentation equilibrium runs were performed at 0.30 mg/mL ErbB3-ECD^L in PBS at 20 °C and rotor speeds of 10,000, 12,000, and 15,000 rpm, again using a Beckman Optima XL-A analytical ultracentrifuge and absorption optics at 280 nm. A partial specific volume of 0.712, calculated as described above, was used. Individual scans were analyzed using the Beckman Origin-based software (Version 3.01) to perform a nonlinear least-squares exponential fit for a single ideal species to give the weight-average molecular weight.

Native Urea Gel Electrophoresis. ErbB3-ECD or ECD^L [2 μM] was incubated in PBS with 5% glycerol for 15 min at 4 °C. A total of 1.6 μg of protein was loaded on a 7.5% Tris-HCl polyacrylamide gel containing 2 M urea. The samples were subjected to electrophoresis in native running buffer (12.5 mM Tris, 96 mM glycine, pH 8.7) at 4 °C for 7 h at 70 mA and stained with coomassie blue. For native gels without urea, ECD^L [2 μM] was treated as above and subjected to electrophoresis on 4−15% Tris-HCl gels (Bio-Rad).

Mass Spectrometry. For MALDI-TOF analysis, working solutions of ErbB3-ECD and ECD^L (1μM, PBS) were diluted 1:1 with α-sinapinic acid (10 mg/mL, 70% acetonitrile, 0.1% trifluoroacetic acid) and dried on a sample plate. The sample was analyzed on a MALDI time-of-flight instrument (Applied Biosystems, Voyager-DE STR, Foster City, CA) in positive ion mode. For calibration purposes the working solutions were plated on the matrix with BSA and cytochrome C (Sigma) as internal standards.

CNBr Cleavage. The location of the additional disulfide bond was confirmed by cyanogen bromide (CNBr) cleavage of recombinant ErbB3-ECDs, followed by Western blot detection of the C-terminal V5 epitope tag or direct visualization after staining with SYPRO-ruby protein stain (Molecular Probes, Eugene, OR). For CNBr cleavage, purified ECDs (2 μg) were treated with 5 mg CNBr (Sigma) in 200 μL 70% formic acid. The reaction mixture was incubated in the dark at room temperature for either 4 or 16 h. The cleavage reaction was terminated by adding two volumes of *N*-ethylmorpholine (Sigma) on ice followed by acetone precipitation. Portions of the precipitated proteins were subjected to separate SDS−PAGE analysis for either direct staining with SYPRO Ruby or Western blot analysis with anti V5 antibodies, conjugated to horseradish peroxidase (Invitrogen, Carlsbad CA).

Surface Plasmon Resonance (SPR). Binding experiments were performed with the surface plasmon resonance-based biosensor instrument BIAcore 3000 (BIAcore AB, Uppsala, Sweden) at 25 °C. Trx-hrg (100 nM) in HEPES (25 mM, pH 6.0) was immobilized on a BIAcore CM5 chip using NHS/EDC amine coupling. Trx-hrg was coupled to flow cell one, and ECD coupling was quenched with ethanolamine. Flow cell two was modified only with ethanolamine, and the final difference in response units (ΔRU) between flow cells was 1400. Injections at various different flow rates and multiple protein concentrations were used to confirm that mass transfer effects were minimal. The final measurements presented in the figures were done in either duplicate (pH dependency analysis) or triplicate (initial measurements for all constructs at physiological pH). Samples were injected at a volume of 35 μL injections at 50 nM ECD (unless stated otherwise) at a flow rate of 5 μL/min. For measurements of the kinetic parameters as a function of pH, the samples (500 nM) were dialyzed in saline (150 mM NaCl, 2.5 mM KCl), then diluted 1:10 with PBS (150 mM NaCl, 2.5 mM KCl, 81 mM Na_2HPO_4, 14.7 mM KH_2PO_4), previously titrated to various pH values (5.0−8.0). Test dilutions on a larger scale confirmed that 1:10 dilutions were sufficient to buffer the solution at the desired pH.

In-Solution Pull-Down of Trx-hrg with Immobilized ErbB3-ECD. For pull-down studies, different ECDs were immobilized on protein A/G agarose using the C-terminal V5 epitope tag and anti-V5 antibodies. A master mix of protein A/G agarose (Santa Cruz Biotechnology, Santa Cruz CA) and V5 antibody (Invitrogen, Carlsbad CA) at a final concentration of 30 μg/mL were incubated for 2 h at room temperature. The resin was washed with PBS (3 × 1 mL) and aliquoted into 0.5 mL centrifugal filter spin-tubes (Amicon Bioseparations, Bedford, MA), each containing 1 μg of antibody coupled to 33 μL equivalents of the original resin slurry. Each aliquot received 1.5 pmol of ECD at a final concentration of 10 nM or PBS for the control. The final slurry was washed with PBS titrated to either pH 7.4 or pH 5.5, and aliquots were incubated with different concentrations of trx-hrg (0.4, 1.5, 3, 9, 18, 30, 90, 270, 400, and 600 nM). To avoid ligand depletion at low concentrations, the volume of the reaction was increased to 10 mL. Based on preliminary tests, the incubation time was increased to 12 h at 4 °C due to the slower rate at which the more dilute reaction reaches equilibrium. The samples were washed three times with 10 mL of PBS (either pH 5.5 or 7.4) at 4 °C. The washed resin was incubated with SDS loading buffer, heated at 95 °C for 10 minutes and samples were run on 4−15% gradient gels. The S-tag containing trx-hrg fusion protein was visualized with S-protein-HRP (Novagen, Madison WI) after transfer to a PVDF membrane (Pierce, Rockford IL), and binding was evaluated by by densitometry. Binding data were directly fitted to a binding model of type $f(x) = B_{max}x/(K_D + x)$ using Origin data analysis software.

Biotinylation of Free Cysteines and Activation of ErbB3/ErbB2 Chimera. CHO/dhfr(−) cells (ATCC) were stably transfected with a Tet-Off control plasmid that also contains tetracycline controlled puromycin resistance (*45*). Stable CHO/Tet-Off cells were transiently transfected with a pIND-TRE-based construct harboring V5 epitope-tagged ErbB3/ErbB2 chimera or ErbB3^L/ErbB2 (Y246C:V574C) chimera (*34*). Transfections were carried out using the Lipofectamine Plus reagent (Invitrogen). For tyrosine phosphorylation assays, cells were serum starved for 16 h in serum-free α-modification of Eagle's medium, 24 h after transfection. Cells were stimulated for 15 min at 37 °C by the addition of 10 nM heregulin-β1 EGF domain (R&D Systems) and were subsequently lysed in SDS−PAGE sample buffer (75 mM Tris-HCl, 10% w/v glycerol, 3% w/v SDS, 2.4 mM bromophenol blue with or without 52 mM dithiothreitol). Lysates were separated on 4−15% gradient gels (Bio-Rad), transferred to PVDF membranes, and probed with either anti-V5-HRP (Invitrogen) or HRP conjugated anti-phosphotyrosine antibody (4G10, Upstate Biotechnology, Inc.).

For cellular biotinylation studies, the transiently transfected cells were incubated with 60 μM PEO-iodoacetyl biotin (Pierce) in PBS, supplemented with 1 mM $CaCl_2$ and 5 mM $MgCl_2$, for 45 min at 25 °C in the dark. Following biotinylation, the cells were washed three times with magnesium and calcium supplemented PBS and lysed in lysis buffer (1% SDS, 5 mM imidazole, 500 mM NaCl, 20 mM Tris, pH 7.9, 1 mM phenylmethylsulfonyl fluoride, 1 mM sodium orthovanadate, 1 μg/mL leupeptin, 1 μg/mL aprotinin, 52 mM dithiothreitol), passed through a 26 gauge needle, heated at 37 °C for 10 min, and centrifuged for 5 min (10000*g*). The supernatant was applied to 0.22 μm centrifugal filters (Millipore Corporation). The filtrate was diluted 1:10 with PBS containing 0.1% SDS and incubated with 100 μL of a slurry of streptavidin agarose (Pierce) for 1 h at 25 °C, washed with PBS/0.1% SDS and eluted with SDS−PAGE sample buffer. The samples were run on 4−15% gradient gels (Bio-Rad), transferred to PVDF membranes, and probed with anti-V5−HRP (Invitrogen). As a positive control for the biotinylation reaction, cell lysis and biotinylation were reversed, giving the biotinylation reaction access to cytoplasmic cysteines. Samples for the control reaction were lysed in lysis buffer without DTT, and biotinylation was carried out for 45 min at 25 °C in the dark with 60 μM PEO−iodoacetyl biotin in PBS plus 1 mM $CaCl_2$, 5 mM $MgCl_2$, and 0.1% [w/v] SDS. Free biotin was removed by acetone precipitation, and the precipitated pellet was redissolved in lysis buffer and processed as described above.

RESULTS

Design of the Constitutively Locked Mutant. The constitutively locked version of the ECD of ErbB3 was designed by introduction of a disulfide bridge between domains II and IV in the area identified as the tether in the crystal structure of ErbB3-ECD (Figure 1, bottom). Suitable residues for replacement with cysteines were evaluated based on the ability to recreate a S_i-S_j distance and $[C_\alpha-C_\beta-S]$ angle for the resulting disulfide bridge that was closest to native disulfide bonds (2.02 Å and 114° respectively (*46*)). Distances and angles were predicted using the software package "O" (*47*). Two pairs of substitutions, L245C−A577C (3.4 Å, 114°) and Y246C−V574C (2.01 Å, 112°), were predicted to have suitable properties. The L245C−A577C double mutant was expressed efficiently in S2 cells but was inefficiently secreted. The Y246C−V574C double mutant showed good expression and secretion and was used for the subsequent analysis. Evaluation of the crystal structure of the locked form of ErbB3 also indicates that both residues in Y246C−V574C are distant from other cysteines in domains II and IV, thereby making incorrect disulfide bond formation less likely. The resulting, constitutively locked ECD will from hereon be referred to as ECD^L.

The Locked Mutant Assumes a Native Conformation. The ECD of ErbB3 contains fifty cysteines forming an intricate network of cysteine knots. In the case of the constitutively locked mutant of ErbB3-ECD, we introduced two additional cysteines and incorrect folding is likely to result in mispairing and the formation of incorrect disulfide bonds between receptors upon storage. Neither freshly isolated ECD^L nor ECD^L that was stored concentrated (3 μM) for several days at 4 °C formed dimers or aggregates as judged by SDS−PAGE in the presence or absence of DTT. Under both conditions, ECD^L and wild-type ECD show an essentially identical running behavior (Figure 2A).

Incorrect formation of intramolecular disulfide bonds is expected to correlate with significant misfolding and a protein that is likely to show reduced solubility. The available crystal structures of either the extended or locked conformation indicate that, despite the significant change in tertiary structure, the formation of the lock is largely the result of rigid body movements with respect to domains I and III and

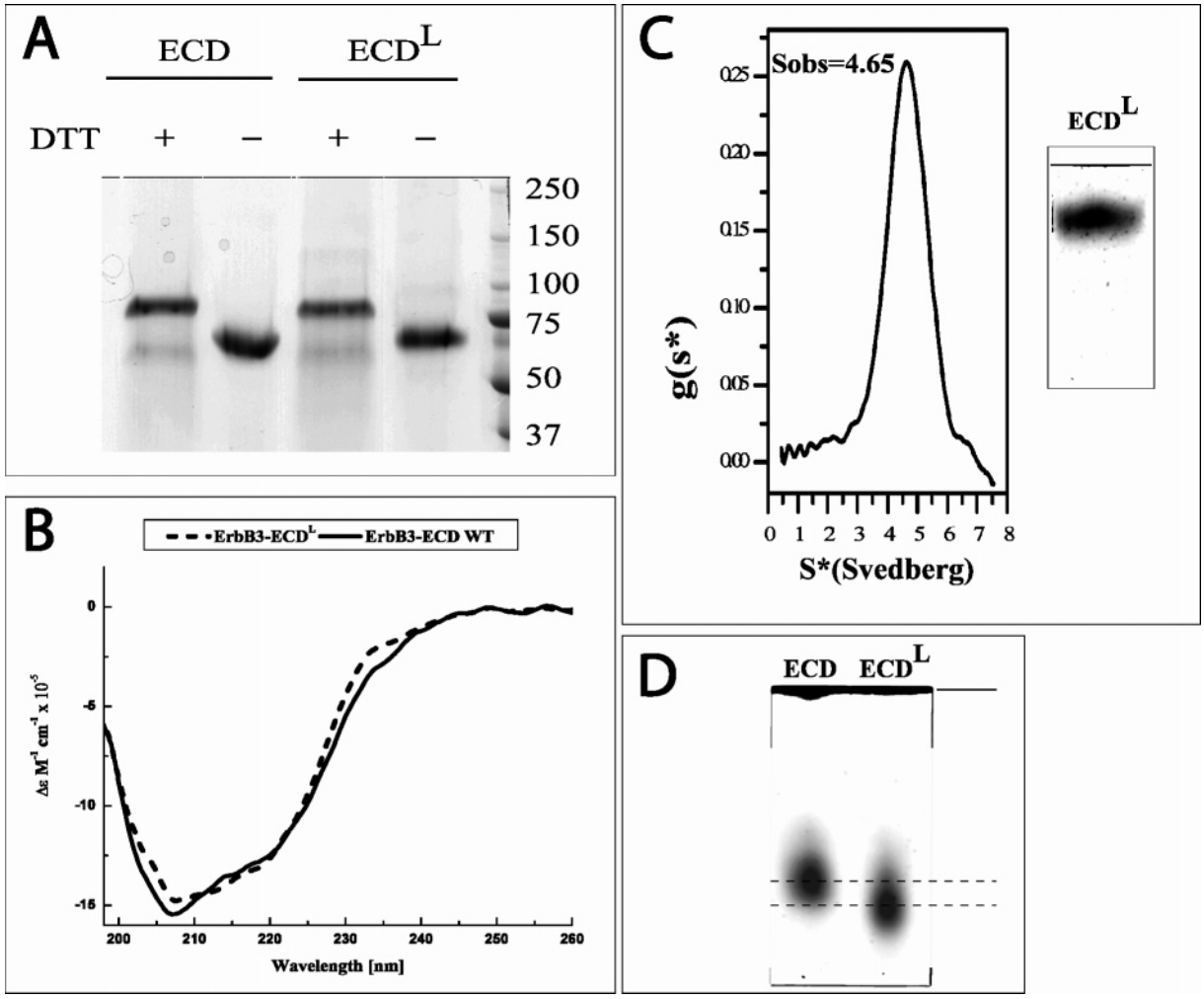

FIGURE 2: ECD^L is correctly folded and monomeric. (A) Coomassie stained SDS−PAGE gel of ErbB3-ECD and ErbB3-ECD^L in the presence (+) or absence (−) of DTT. (B) Circular dichroism spectra of ErbB3-ECD (solid trace) and ErbB3-ECD^L (dashed trace). (C) (Left): Ultracentrifugation velocity analysis shows a single dominant species (>90%) with a sedimentation behavior that is consistent with monomeric ECD^L. (Right): ECD^L runs as a single band in a native PAGE gel. The black line indicates the position of the gel-loading pocket. (D) ECD^L shows enhanced electrophoretic mobility in a urea supplemented native gel, without changes in mass or charge, indicating a more compact molecule.

most of domains II and IV. As a consequence, ECD^L would be expected to have a very similar secondary structure composition to wild-type ECD. We therefore compared the circular dichroism spectrum for ECD^L and wild-type ECD. Both ECDs show very similar CD spectra (Figure 2B). However, ECD^L does show a noticeable change in the spectrum at 210 and 230 nm, indicating some loss of secondary structure and increase in random coil content, probably due to strain placed on the first segments of domains II, III, and IV resulting from the loss of part of the interdomain interfaces compared to the extended wild-type structure. This lack of stabilization at domain interfaces is also reflected in the crystallographic *B*-factor distribution of the locked ECD of ErbB3 compared to the ECD of ErbB2 in the extended conformation. While the extended ErbB2 ECD shows fairly uniform *B*-factors (*23*), ErbB3-ECD in the locked conformation shows a more nonuniform distribution of crystallographic *B*-factors, indicating a higher degree of local flexibility. Pronounced areas with elevated *B*-factors are the β-sheets at the N and C-terminal ends of domain III, which is missing some of the interdomain contacts compared to the extended conformation (*25*). However, overall the CD spectra are consistent with two structures with significantly different tertiary structures, but very similar secondary structures. Taken together, these findings support the assumption that the structure-based introduction of the double mutation Y246C−V574C does result in a properly folded ECD.

Incorrect folding is also likely to result in a protein with compromised solubility. While we previously demonstrated that wild-type ECD at elevated concentrations readily forms oligomers (*41*), ECD^L is expected to be largely monomeric, since oligomerization proceeds from the extended conformation of the ECD (*34*). We therefore analyzed ECD^L with respect to its behavior in native gel electrophoresis as well as analytical ultracentrifugation. Even at elevated concentrations (2 μM), ECD^L runs as a single band in a native PAGE gel (Figure 2C, right panel), and shows a (>90%) homogeneous peak at 0.3 mg/L in an ultracentrifugation run with less than 5% of the sample showing slower sedimentation behavior and a comparable percentage showing marginally faster sedimentation (Figure 2C, left panel). This dominant species was estimated to represent a molecule of a molecular mass of 77 kDa by equilibrium ultracentrifugation, compared to a molecular mass of 79 kDa for the monomer by MALDI-TOF.

Since the double mutation in ECD^L does not alter the net charge of the protein, we reasoned that the locked conformation should result in a considerably more compact molecule, which may be detectable by comparing its running behavior to that of wild-type ECD in native gel electrophoresis. To ensure that the mutagenesis did not result in a change in the amount of attached carbohydrate we determined the molecular mass of ECD and ECD^L by MALDI-TOF. This analysis revealed essentially identical mass estimates for both constructs (80 (±4) and 79 (±5) kDa, respectively, with standard deviations reflecting peak width). Although ECD^L is monomeric by ultracentrifugation with only a very small component of dimers (<5%), the wild-type ECD readily oligomerizes. To eliminate the impact of protein interactions, especially for the wild-type ECD, we carried out this analysis in the presence of 2 M urea, which is sufficient to disrupt protein interactions but will not denature the protein (*34*). Under those conditions, ECD^L does indeed show a higher electrophoretic mobility, indicating a more compact structure (Figure 2D). This can be observed despite the fact that the carbohydrate chains, making up 18% of the mass, are likely to protrude significantly from the body of both ECDs, diminishing the shape effect. Attempts to evaluate both constructs in the presence of reducing reagents on urea supplemented native gels resulted in aggregates of both species, probably due to the loss of secondary structure for the reduced domains II and IV in the presence of urea and in the absence of the stabilizing 25 or 26 disulfide bridges.

In order to further confirm that the engineered disulfide bridge formed between the correct disulfides, we evaluated the CNBr induced fragmentation pattern of the extracellular domains in the presence and absence of reducing reagent. All of the 50 cysteines in the extracellular domains of ErbB3 form close-range disulfide bridges, mainly as part of the cysteine knot configuration of domains II and IV. In contrast, the formation of the additional disulfide bridge between residues 246 and 574 of ECD^L generates a long-range disulfide bridge that can be distinguished after fragmentation of the ECD under oxidizing conditions (Figure 3A). We initially attempted the analysis of fragments obtained by tryptic digest, but the compact nature, especially of domains II and IV, did not allow for efficient tryptic digestion without prior reduction of the 26 disulfide bridges in ECD^L. In contrast, complete cleavage could be obtained with CNBr, and the anticipated fragmentation pattern is shown in Figure 3A together with the domain structure of the ECD. Five major fragments represent most of the mass of the extracellular domains (79%). In wild-type ECD, they are held together by disulfide bridges to form a 28.7 kDa segment I (fragments 4, 5, and 7) and a 24.6 kDa segment II (fragments 9 and 10, including the C-terminal V5 epitope). This mass estimate does not include the additional 10 kDa of carbohydrate attachments which result in a shift toward higher aberrant molecular weights on SDS−PAGE gels (*41*).

The formation of the correct disulfide bridge between segments I and II can be detected by tracking the V5 epitope tag at the end of segment II (fragment 10). Cyanogen bromide cleavage of wild-type ECD for 4 h results primarily in the production of a dominant band with an apparent molecular weight around 33 kDa (marked ▼ in Figure 3B), likely to represent segment II (fragments 10 and 9: expected potein mass = 24.6 kDa), including most of the carbohydrate

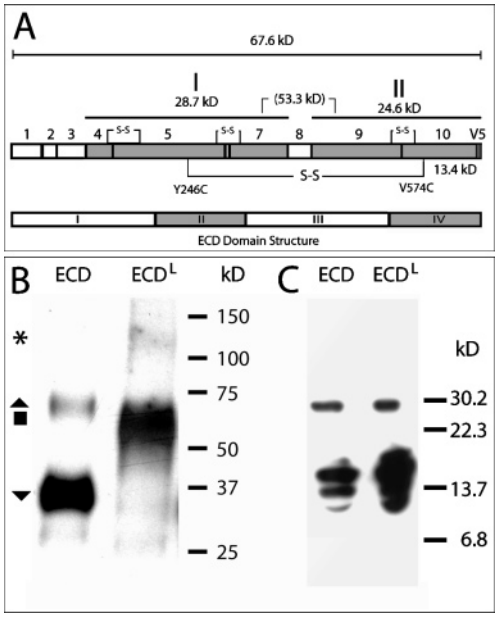

FIGURE 3: The Y246C and V574C double mutant forms a long-range disulfide bridge, consistent with a disulfide-bridged tether. (A) Map of peptides (1−10) that are anticipated from the CNBr cleavage of the ErbB3-ECD and location of the V5 epitope tag. The location of critical disulfide bridges that link fragments are indicated. The sizes of segments I (fragments 4, 5, and 7), II (fragments 9 and 10), the anticipated molecular weight for linked segments I and II as well as full-length ECD are given without the mass contributed by carbohydrate. The domain structure of the ErbB3-ECD is shown below for reference purposes. (B) CNBr digest of ECD and ECD^L and visualization of the running behavior of fragment 10 by Western blot detection of V5 epitope after SDS−PAGE analysis in the absence of DTT. The gel shows the results of the 4 h digest for ECD and overnight digest for ECD^L. Relevant bands are marked to the left for reference purposes. (C) Fragments produced by a 4 h CNBr digest of reduced ECD and ECD^L, visualized by Western blot analysis with anti-V5 antibodies after SDS−PAGE analysis in the presence of DTT.

component. A residual full-length band remains (▲), showing an apparent molecular weight around 75 kDa under nonreducing conditions. ECD^L digestion after 4 h showed a larger fragment. To ensure that this was not the result of incomplete cleavage, we subjected ECD^L to prolonged overnight cleavage (Figure 3B). Even after overnight CNBr cleavage, the primary band obtained with ECD^L (■) does not correspond to the smaller molecular weight band observed for wild-type ECD, but instead shows an apparent molecular weight that is slightly smaller than full-length ECD, consistent with the anticipated molecular weight of the combined segments I and II (67.6 kDa plus carbohydrate) and the formation of a long-range disulfide bridge between fragments 5 and 10. The Western blot also reveals a small fraction of ECDs that have instead formed dimers in solution (*). Traces of an even smaller fraction of individual segment II is visible, representing ECDs that either failed to form the lock or misfolded entirely. We estimate both fractions to be below 0.1% of the total receptor ECDs.

Analysis of the cleavage products under reducing conditions (after 4 h of digest) shows matching digestion patterns for both constructs (Figure 3C), with the dominant bands around 13−14 kDa, the molecular mass of the V5 epitope carrying fragment 10 (13.4 kDa, without carbohydrate). A minor band around 30 kDa is likely to represent incomplete cleavage between fragments 9 and 10 in both cases but is

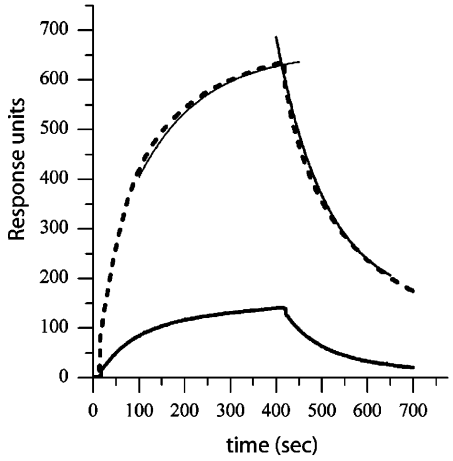

FIGURE 4: Surface plasmon resonance analysis of the binding of ECD^L to immobilized trx-hrg at a fixed pH of pH 7.4 and two concentrations of ECD^L (10 and 50 nM). The sensorgram for 50 nM ECD^L is shown with the fit for a 1:1 Langmuir dissociation and association using an on-rate of 9.0×10^4 (1/(M s)) and off-rate of 3.95×10^{-3} (1/s) giving a K_D estimate from this single run of 44 nM. K_D values shown in Table 1 are the results of measurements in triplicate at the indicated concentrations.

equally present in both digests. The identical fragment pattern under reducing conditions confirms that the differences seen under oxidizing conditions are not due to qualitative difference in the cleavage pattern of ECD and ECD^L but are the result of the engineered, long-range disulfide bridge.

The Locked ECD Binds Heregulin with an Affinity Comparable to That of the Individual Domains I and III. We evaluated ligand binding by SPR as well as saturation binding studies, using a pull-down assay. For SPR, we immobilized a fusion protein (trx-hrg), consisting of thioredoxin and the EGF-like domain of heregulin β1, to the surface of a surface plasmon resonance chip. The trx-hrg fusion protein was previously shown to have comparable affinity for both the recombinant ECD and the receptor on cell surfaces. The use of the fusion protein also protects the essential and unique lysine at the N-terminus of the EGF-like domain of heregulin from chemical modification, by instead favoring the immobilization via the larger fusion protein component. Table 1 summarizes the binding constants obtained by SPR from measured on- and off-rates at ECD concentrations of 50 nM and lists binding constants reported in the literature, where available. In our SPR study, ECD^L exhibits strong binding to the immobilized ligand with a K_D of 52 nM (Figure 4). This relatively strong affinity is nevertheless reduced compared to the affinity of wild-type ECD (5 nM) or the 1 nM K_D of the previously described extended mutant H565F (ECD^E). In ECD^E, a hydrogen bond, which is critical for the stabilization of the intramolecular lock, has been eliminated. Hence, both wild-type ECD and ECD^E bind ligand with more than 10-fold higher affinity than ECD^L.

Next we compared the ligand binding by ECD^L to that of the individual domains I and III. As domains I and III do not express stably as self-standing domains, both were expressed in conjunction with domains II and IV which follow immediately at their respective C-termini and share a significant interface with either domain I or domain III. Based on SPR measurements, both partial ECD constructs (ECD^{I-II} and ECD^{III-IV}) showed relatively strong binding which was comparable to the binding observed for ECD^L.

ECD^{III-IV} Shows Aberrant Binding Behavior in SPR Studies. The strength of SPR lies in its ability to derive K_D estimates in a single measurement and the fact that it gives direct access to dissociation on-rates and off-rates. The most common causes for artifacts in these measurements are mass transfer effects due to overloaded or otherwise improperly prepared chip surfaces or insufficient flow rates. Under those conditions the kinetics of ligand supply can become limiting or excessive rebinding of dissociated ligand can result in apparently reduced off-rates. In the case of wild-type ECD we were able to validate the measured affinities by comparison with previously published data. As is shown in Table 1, the observed affinity is in good agreement with the majority of affinities reported elsewhere. This suggests that the procedure used to immobilize the ligand did not compromise activity. Since all other ECDs were evaluated against the same chip, carrying moderate amounts of immobilized ligand, this source of artifacts can be ruled out for all constructs. When the ECD is immobilized (data not shown), this assumption is not true, since the nature of the immobilization reaction can significantly reduce the ligand affinity of the ECD, and this effect will vary greatly between ECDs and different immobilization reactions.

When calculated arithmetically from estimated on- and off-rates of individual runs, and assuming sufficient signal can be obtained, the same dissociation constant should be obtained for a given ECD, regardless of the concentration of the ECD that was passed over the chip surface or the flow rate at which the measurement was carried out. We applied this internal test to the affinity measurements done for all ECD constructs. Under different conditions, comparable results were obtained for all but one construct with minimal variations between duplicate runs. The only construct which showed deviations as a function of ECD concentration was ECD^{III-IV}. While K_D values for ECD^{III-IV} obtained at a given concentration of ECD showed variations of less than 10%, K_D values obtained at different concentrations of ECD^{III-IV} were markedly different, ranging from 9 ($\pm$3) to 90 ($\pm$6) nM when measured at 50 and 100 nM ECD, respectively. No interpretable data could be obtained at 400 nM. These changes are largely due to variations in the on-rate, and the higher concentrations correspond to conditions under which ECD^{III-IV} in our hands begins to show strong indications of aggregation upon storage. In contrast, ECD^{I-II} yielded binding constants of 49 ($\pm$3) and 52 ($\pm$4) nM under the same conditions. While subsequent pull-down studies qualitatively confirmed the binding properties of ECD^{III-IV} compared to ECD^{I-II}, the absolute binding constant obtained for this particular construct ought to be interpreted with caution.

The Locked and Extended Conformation Retains Ligand Binding at pH 5.5. One intriguing characteristic of the documented crystal structure of EGFR-ECD in a locked conformation with bound ligand is the fact that it was obtained at pH 5.0. The observed binding to domain I of EGFR had been interpreted as low affinity binding, forced by high ligand concentrations under conditions at which the primary binding site in domain III is nonfunctional due to protonation of critical histidines (*26*). Our previous work had indicated that, in contrast to EGFR, domain I of ErbB3 is a significant contributor to binding (*27*). We therefore tested

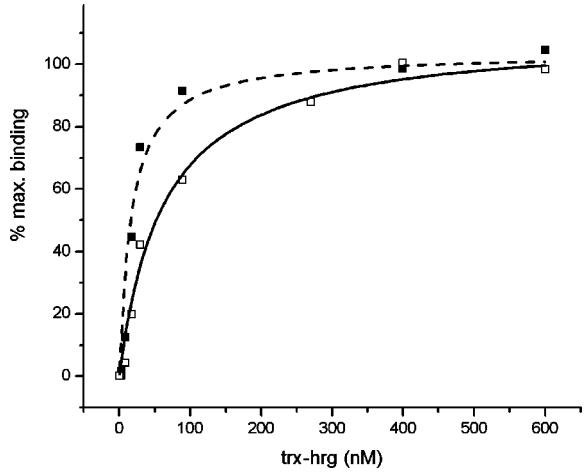

FIGURE 5: In-solution pull-down assays confirm strong binding of heregulin to ECD^L at pH 7.4 and 5.5. The pH dependent binding of trx-hrg was measured in a pull-down assay with V5-tagged ErbB3-ECD^L at pH 7.4 (□, solid line) and pH 5.5 (■, dashed line). Bound trx-hrg was detected with S-protein-hrp conjugate and is presented as a function of ligand concentration and percentage of maximum binding.

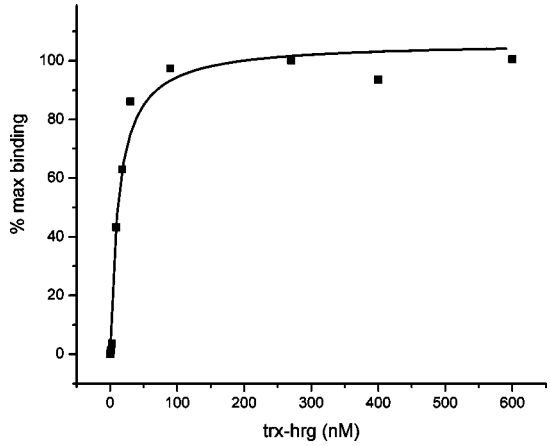

FIGURE 6: Wild-type ECD retains strong binding of heregulin at pH 5.5. The ligand binding of immobilized wild-type ECD was determined with a pull-down assay at different concentrations of trx-hrg. Bound trx-hrg was detected with S-protein-hrp conjugate. The percentage of maximum bound ligand is plotted as a function of ligand concentration.

if we could observe binding to ECD^L at low pH and physiologically relevant ligand concentrations. We evaluated the binding of trx-hrg to ECD^L at pH 5.5 versus 7.4 using a conventional in-solution pull-down assay at different concentrations of ligand. This study has an inverse configuration to the SPR studies in that the ECDs are immobilized and the binding of ligand is measured. The saturation binding curve obtained in this study (Figure 5) indicated a binding constant for ECD^L at pH 7.4 of 65 nM. Despite the reversed setup of the assay, this in good agreement with the measurement obtained by SPR (52 nM). Surprisingly, ECD^L not only retained binding at pH 5.5 but showed a modest increase in affinity (25 nM) in this assay.

The finding of strong binding of heregulin to the locked ECD at pH 5.5 was unexpected and in contrast to the model for purified EGFR-ECD which has been reported to lose ligand binding affinity at endosome pH (*26*). We therefore evaluated if wild-type ECD would also retain ligand binding at endosome pH, using a pull-down study and conventional saturation curve analysis (Figure 6). This analysis yielded an estimate for the binding constant at pH 5.5 of 13 nM, indicating that both conformations of ErbB3 are distinct from EGFR in their ability to retain ligand binding at endosome pH.

The pH Dependency of Binding by ECD^L Is Mirrored by the Binding Behavior of ECD^{I-II}. Since the binding constant of 52 nM for ECD^L obtained by SPR at neutral pH is in good agreement with the K_D estimate obtained by pull-down assays at pH 7.4 in a reversed configuration (65 nM), we carried out a systematic evaluation of the impact of pH on ligand binding for all constructs using SPR. The analysis of binding by SPR facilitates the evaluation of a larger set of conditions, primarily due to a greatly reduced requirement for the amount of purified receptor and ligand needed for the assays. This was especially a concern for ECD^{III-IV}, which was available in limited supply and is prone to aggregation at elevated concentrations, complicating conventional saturation binding studies. In order to limit the effect of self-association of ECD^{III-IV} on measurements, all data were obtained at 50 nM. At this concentration ECD^{III-IV} is well below its threshold for aggregation and robust SPR signals could be obtained for all constructs.

We evaluated the impact of pH on ligand binding for all five constructs at seven different pH values, ranging from pH 5.0 to 8.0. Figure 7 shows a graphical representation of the impact of pH on the overall K_D, as well as the dissociation on-rate and off-rates. The representation of the calculated K_D values of the three full-length constructs as a function of pH (Figure 7a) also shows that ECD^L maintains ligand binding at low pH. Using SPR as the readout, the increase in binding affinity is more pronounced and reveals a minimum at pH 5.5 (1.7 nM, ±0.4). In the case of wild-type ECD, the pH minimum is slightly shifted to pH 6.0, but the binding constant 12 (±2) nM obtained by SPR is in very good agreement with the result obtained by pull-down studies (13 nM).

SPR and pull-down studies qualitatively confirm an increase in affinity for ECD^L at low pH, and specific K_D values obtained by both methods are in good agreement in the case of ECD^L at pH 7.4 (52 versus 65 nM) and wild-type ECD at pH 5.5 (12 versus 13 nM). However both methods differ in the specific K_D values, obtained for ECD^L at pH 5.5 (2 nM by SPR versus 25 nM in the pull-down study). The reason for this discrepancy is not clear but may be related to the mode of immobilization. Our data indicate that binding by domain I is dominant at pH 5.5 but not pH 7.4. In the case of ECD^L, but not wild-type ECD, the relevant binding interface of domain I is brought in close proximity of the C-terminus, which serves as the point for antibody-based immobilization in the pull-down methods, thus potentially resulting in interferences with ligand binding. In the case of SPR studies, the ligand, not the ECD, is immobilized, eliminating this ECD construct specific interference.

An intriguing feature of the pH profile of all three full-length ECDs is the presence of contrary pH minima for ECD^L and ECD^E as well as the absence of a pronounced minimum for wild-type ECD (Figure 7a). While ECD^L binding shows a single and pronounced minimum at pH 5.5, ECD^E shows a minimum, although less pronounced, at pH 7.4. By comparison, wild-type ECD shows a more uniform binding

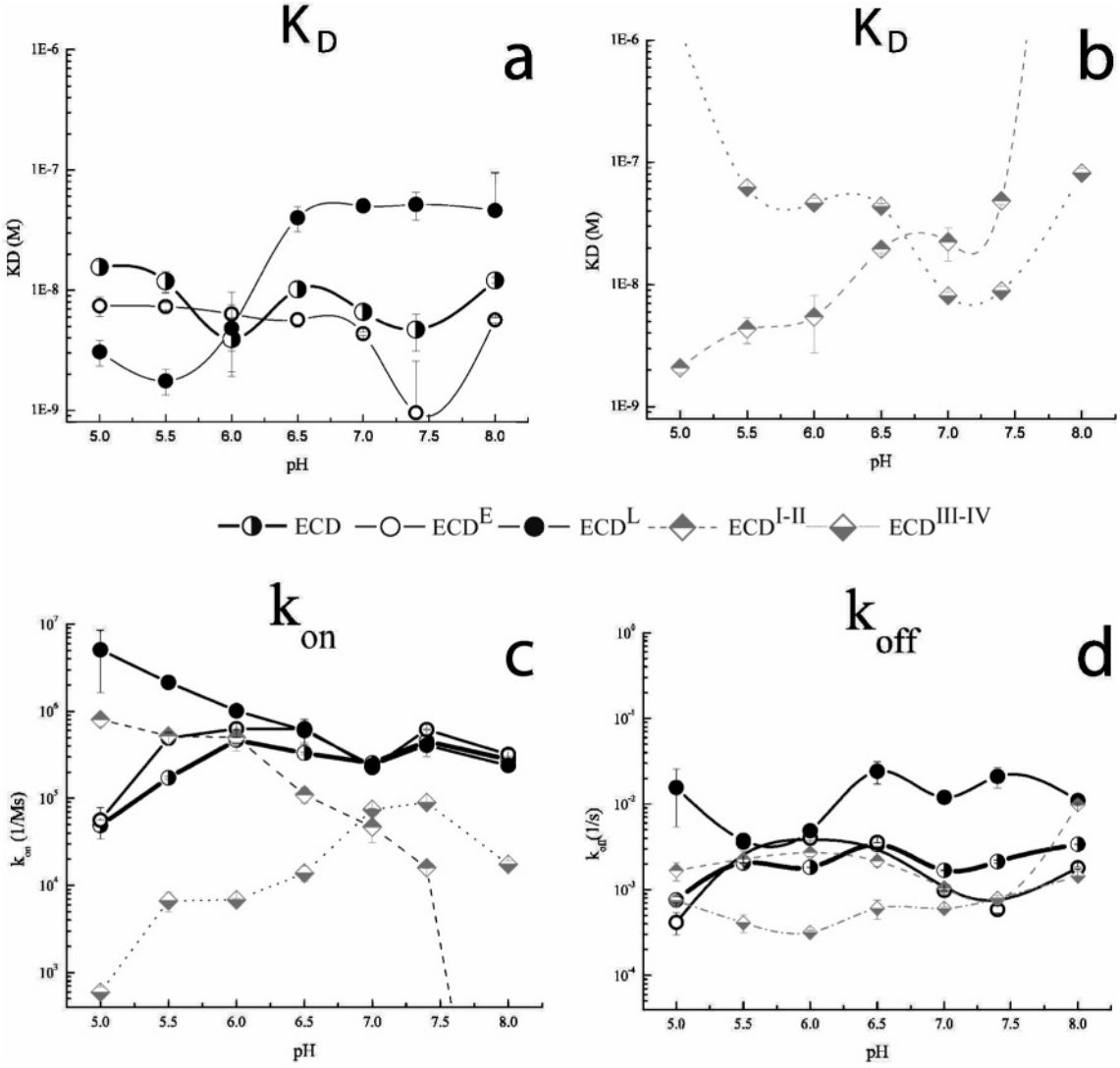

FIGURE 7: ErbB3-ECD binding parameters as a function of pH, measured by SPR. The binding of different ECD constructs (indicated above plots) to immobilized trx-hrg was measured at 50 nM ECD and various pH values. The estimated K_D values are given for the three full-length constructs (ECD, ECD^E, and ECD^L, panel a) and the half constructs (ECD^{I-II}, ECD^{III-IV}, panel b). The on-rate is given in panel c on the same log scale as the off-rate, presented in panel d.

behavior over the same pH range with two shallow minima at 6.0 and 7.4. This more uniform binding behavior as well as the dual minimum would be consistent with the assumption that the wild-type ECD exists in an equilibrium of both conformational states. However, more direct measurements of the presence of these alternative conformational states would be needed to confirm the presence of such an equilibrium as well as the relative proportion of receptors in the respective locked and extended conformations.

ECD^{I-II} and ECD^{III-IV} Respond in a Contrary Fashion to a Shift in pH. While both wild-type ECD and ECD^L maintain binding affinity at endosome pH, the SPR data on ECD^{I-II} and ECD^{III-IV} suggest that this net retention is the result of alternating contributions of domains I and III at different pH values (Figure 7b). Overall, the binding behavior of ECD^{III-IV} qualitatively mirrors that of ECD^E with a minimum between 7 and 7.4 and a decrease in binding at lower pH. In contrast, ECD^{I-II} shows reduced binding at physiological pH and a gain in affinity as the pH is decreased. A comparison of dissociation on- and off-rates indicates that most of the changes occur on the part of the dissociation on-rates, shown in Figure 7c on the same log scale as the dissociation off-rate in Figure 7d.

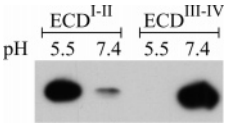

FIGURE 8: Immobilized ECD^{I-II} and ECD^{III-IV} show a contrary pH dependency in their binding of heregulin. ECD constructs were immobilized via their C-terminal V5 epitope tag, and bound ligand (trx-hrg) was determined by Western blotting after incubation with 10 nM ligand. The ECD constructs and pH of binding are indicated above the lanes. While ECD^{I-II} shows good binding at pH 5.5 and lower binding at pH 7.4, the inverse is true for ECD^{III-IV}.

We used the pull-down assay to qualitatively confirm the SPR data suggesting a contrary effect of pH changes on the affinity of ECD^{I-II} and ECD^{III-IV}. To this end, dilute partial ECDs were immobilized on resin and ligand binding was measured at either pH 5.5 or 7.4 at a single nonsaturating ligand concentration of 10 nM (Figure 8). Based on the K_D estimates obtained by SPR, this concentration of ligand was expected to maximize the differences in binding between both constructs and at different pH values. Binding under those limiting conditions qualitatively confirms the contrary

binding behavior of each construct as a function of pH. While binding to ECD^{I-II} is increased at pH 5.5, binding to ECD^{III-IV} is decreased and no significant binding was observed at pH 5.5. The inverse is true at pH 7.4, although ECD^{I-II} appears to be more capable of binding ligand to some extent under both sets of conditions. With respect to the aberrant behavior of ECD^{III-IV} in SPR studies, this pull-down study also supports the observation of strong binding by ECD^{III-IV} at pH 7.4, and in fact argues in favor of tighter binding compared to ECD^{I-II}, at least outside of the context of the full-length ECD.

The Disulfide Stabilized Lock Does Not Engage on the Cell Surface. While the above data suggest a possibly enhanced role of the locked conformation at endosome pH, previous mutagenesis studies had questioned the role of this conformation on the cell surface. Since the deprotonated sulfhydryl species is needed for disulfide bridge formation, this mode of stabilization cannot be used if the locked conformation is mainly assumed in the endosome. However, we can address the question if the quantitative formation of the additional disulfide bridge, seen for the secreted ECD, is impaired for the cell-surface anchored receptor. Under the oxidizing conditions of the cell surface, the locked conformation should be stabilized in our double mutant, assuming that the receptor is sterically capable of assuming the locked conformation. As this disulfide bridge is effectively irreversible, this should result in the gradual shift toward the locked species, even if only a modest proportion is present in equilibrium.

To evaluate the formation of the lock on the cell surface we generated a membrane anchored ECD^{L} mutant in the context of an ErbB3−ErbB2 chimera. This previously described chimera (*34*) contains the ErbB2 transmembrane and cytoplasmic portion to obtain tyrosine phosphorylation as an additional readout. We evaluated four properties of the ECD^{L} chimera: expression levels and signs of instability, formation of disulfide linked dimers, constitutive and ligand-induced autophosphorylation, and the presence of free cysteines (Figure 9). Both the chimera containing wild-type ECD (W) and the chimera containing the ECD^{L} domain (L) express stable protein at comparable levels, as judged by the signal of their C-terminal V-5 epitope tag (Figure 9A). Even under conditions of overloading and in the absence of reducing reagent, no indication of disulfide stabilized dimers is present, suggesting that the ECD^{L} chimera exists either in the locked form or with free non disulfide forming cysteines. An analysis of the activity of both chimera shows that chimera with wild-type ECD exhibits the anticipated ability to respond to heregulin while the ECD^{L} chimera exhibits elevated levels of constitutive phosphorylation but fails to respond to ligand (Figure 9B). The lack of response to ligand and the elevated basal activity of the ECD^{L} chimera matches properties of two previously described mutants of EGFR, Y245A, R285S, (*21*) and Y246D (*13*). Of those two dimerization loop mutants in EGFR, Y246D carries a single amino acid mutation in the equivalent position to the Y246C mutation in ECD^{L}.

To distinguish between a constitutively locked and hence inactive receptor and the possibility that the ECD^{L} chimera exists in an extended but non ligand responsive form, we assayed for the presence of free cysteines in the ECD^{L} chimera through derivatization of cell surface receptors with

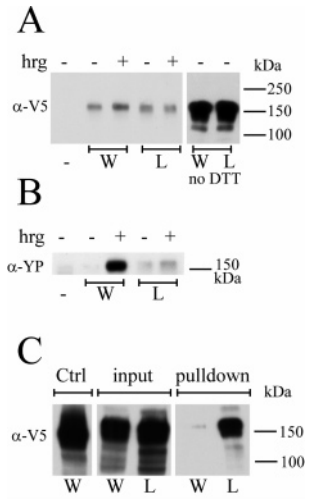

FIGURE 9: The Y246C−V574C double mutant does not form a lock on the cell surface. (A) Chimeric ErbB3/ErbB2 that contain either wild-type ErbB3-ECD (W) or Y246C−V574C double mutant ECD^{L} (L) express at comparable levels, based on a Western blot of the V5-epitope tag (left side with DTT). Even at high exposure levels, no covalent dimers are visible in the absence of DTT for the chimera carrying the ECD^{L} double mutation (right side without DTT). (B) ECD^{L} chimera show enhanced constitutive phosphorylation but fail to respond to heregulin stimulation as judged by an anti-phosphotyrosine Western blot. (C) V5 Western blot of chimera after pull-down with streptavidin agarose. The control reaction (Ctrl) represents wild-type chimera, labeled with PEO-iodoacetyl-biotin after cell lysis. The pull-down lanes represent the fraction of wild type (W) and lock mutant (L) pulled down after labeling on intact cell surfaces. "Input" represents equivalent fractions of lysate that were subjected to the pull-down.

iodoacetyl biotin. As a positive control for the modification reaction (Ctrl) we treated lysates of cells transfected with wild-type ECD chimera following cell lysis. Under those conditions, receptors are expected to be efficiently biotinylated at several unpaired cysteines in the cytoplasmic portion of the receptor. Western blot analysis of the streptavidin pull-down (Figure 9C) confirms that while control lysates were efficiently biotinylated, no significant biotinylation occurred on the surface of intact cells for the chimera carrying wild-type ECD. In contrast, the ECD^{L} chimera was efficiently biotinylated, indicating that the receptor was present on the cell surface, and that the lock had not formed, at least for a large portion of the receptors. Combined findings for cell surface expressed ECD^{L} chimera suggest that the receptor is stably expressed without unwanted intermolecular disulfide bridge formation, but is largely trapped in an extended conformation with activation properties that resemble those of constitutively extended mutants of EGFR with a mutagenized dimerization loop.

DISCUSSION

While multiple crystal structures have shown the existence of a locked or tethered conformation for ErbB receptors, the biological role of this conformation and its relative abundance in an equilibrium of different conformations remains unclear. In order to evaluate the ligand binding properties of the locked conformation, we have generated a constitutively locked version of the ECD of ErbB3 by introducing a disulfide bridge into the tether region between domains II and IV of ErbB3. The constitutively locked ECD shows strong binding of ligand. Surprisingly we also found that

the locked form shows improved binding at low pH. ECD^L shares its ability to retain binding at low pH with wild-type ECD. This binding behavior of ECD and ECD^L is in contrast to EGFR, which loses affinity for EGF at low pH. Qualitatively, the binding behavior of ECD^L best matches that of truncated constructs of the ErbB3-ECD containing only domains I and II (ECD^{I-II}). We previously reported that, in contrast to EGFR, domain I of ErbB3 shows a strong contribution to ligand binding. This distinct contribution by domain I is therefore matched by its ability to impart ligand retention to the full-length ECD at endosome pH.

The Introduction of the Disulfide Bridge in ECD^L Results in Properly Folded ErbB3-ECD with a Correctly Placed Additional Disulfide Bond. The interpretation of ECD^L binding properties assumes proper folding and the efficient formation of the engineered disulfide bridge in the locked conformation. Based on several criteria, ECD^L is correctly folded and stabilized as designed. These criteria include the absence of any significant portion of disulfide linked dimers or higher order oligomers on oxidizing SDS−PAGE and a CD spectrum that is very similar to that of wild-type ECD, despite significant differences in the tertiary structure. The expressed ECD runs as a single band in a native gel, and >90% of the protein behaves as monomeric species with estimated molecular mass of 77 kDa by analytical ultracentrifugation. Without change in charge and with a comparable estimated mass, ECD^L shows accelerated running behavior compared to the wild-type ECD in urea supplemented native gels, indicating a more compact molecule. Furthermore, the binding behavior of the locked species at neutral pH matches expectations for a construct in which the individual domains I and III, known to constitute the bivalent binding pocket in the extended form of the receptor, were separated but individually accessible. This suggests the correct folding of domains I and III. Finally, the correct formation of the engineered disulfide bridge between Y246C and V574C was also confirmed by CNBr cleavage and analysis of the fragments under oxidizing conditions. Together these findings argue that, despite the presence of fifty cysteines in the wild-type receptor ECD, the structure based introduction of an additional disulfide bridge between positions 246 and 574 resulted in a correctly folded and disulfide-bridged ECD in a constitutively locked conformation.

The Locked ECD^L Mutant Shows Binding That Is Consistent with Binding by a Single Interface in Either Domain I or Domain III. We confirmed the binding of the locked mutant to heregulin by two independent assays, surface plasmon resonance and conventional saturation binding studies in a pull-down assay. Both approaches confirmed relatively strong ligand binding at pH 7.4 with K_Ds of 52 and 65 nM, respectively. This binding is approximately 10-fold lower than the binding observed for the wild-type ECD and 50-fold lower than binding by the extended mutant. These results are consistent with the overall predictions based on the model provided by the crystal structure of EGFR with bound ligand. In the extended conformation, the ligand binds in a pocket between domains I, II, and III with domains I and III making critical contacts (*19*, *20*). Contacts by both domains, I and III, have also been demonstrated by cross-linking studies (*28*, *29*). This dual interaction of the receptor with the ligand is disrupted in the locked conformation. Here, the spatial separation between the putative contact regions in domains I and III is too large to permit simultaneous interactions with ligand (60 Å in the case of ErbB3) and the relevant surfaces are also rotated, thus precluding the formation of a joint binding site (*25*). This change is demonstrated in Figure 1 (top) for EGFR where crystal structures for both relevant conformations are available, including bound ligand. The stabilization expected from the simultaneous interaction of two binding sites in the extended conformation is therefore lost, and the affinity observed for ECD^L is more comparable to those observed for the ECD^{I-II} and ECD^{III-IV} constructs.

Given the spatial separation of the two putative ligand interfaces in domains I and III, it is conceivable that the ECD in the locked conformation would be capable of binding two molecules of ligand, albeit with different affinities. The SPR data suggest that the affinities of both interfaces are restively close at pH 7.4, and this is confirmed by the pull-down study which showed strong binding by ECD^{III-IV} and to a lesser extent by ECD^{I-II} (Figure 8). The corresponding K_D values obtained by SPR at pH 7.4 were 9 nM and 48 nM, respectively. In contrast, strong ligand binding could be detected for ECD^{I-II} at pH 5.5 while binding by ECD^{III-IV} was not observed under conditions of dilute ligand (10 nM). This was mirrored by the larger differences in K_D of 4 and 52 nM respectively measured by SPR. However, neither the SPR analysis nor the in-solution pull-down study of ECD^L showed clear indications of a complex mode of binding. However, this absence of a complex binding behavior may simply reflect limitations of the techniques, especially in the pull-down studies where the available number of data points is insufficient to detect two relatively similar K_Ds.

Binding of Heregulin by the Extended Monomeric Receptor Involves "Partial Bivalency". Several lines of evidence support a bivalent mode of binding of heregulin to ErbB3. Bivalent in this context refers to a binding mode that utilizes contributions of domains I and III to the overall affinity of the ligand receptor complex. At pH 7.4, both individual interfaces show binding by SPR and pull-down studies. Under those conditions, the affinity of wild-type ECD and ECD^E exceeds that of ECD^{I-II}, ECD^{III-IV}, and ECD^L. Another indication for a bivalent mode of binding is provided by the strength of ligand binding by ErbB3 compared to EGFR. The binding constant obtained at pH 7.4 for the full-length ECD in this and previous measurements (*27*) is in good agreement with most of the measurements for both the purified ECD and cellular ErbB3 which are in the range of 1−10 nM (Table 1). This is significantly stronger than the interaction reported for the binding of EGF to purified EGFR-ECD (500 nM (*30*)). This higher affinity may reflect the fact that ErbB3 has a considerable binding contribution from domains I and III while binding of EGF to EGFR involves contacts to both domains but the binding energy has been largely attributed to interactions made only by domain III.

While we qualitatively observed the increase in affinity that would be expected from a bivalent interaction of the ligand with domains I and III, the available data also suggest that the full potential of this bivalent mode of binding is clearly not realized. For different pH values the binding observed by wild-type ECD traces more closely with that of the extended form of the receptor than the locked form, although to a lesser extent at pH 5.5. This suggests that most of the wild-type receptor is in an extended and not in a locked

conformation. Assuming that no additional constraints are imposed by the structure of the extended conformation and both interfaces contribute fully to binding, one would anticipate extremely tight binding of ligand to the extended receptor on the order of 10^{-15} M. Clearly this affinity was not observed for the extended receptor nor would such tight binding be biologically useful for the interaction of a growth factor with its target receptor. Furthermore we observed that, at least at pH 5.5, the affinity of ECD^{I-II} and ECD^{L} exceeds that of wild-type ECD and ECD^{E}, which is not possible if both binding sites contribute fully to the overall binding. Together this suggests that a simple bivalency model does not fully describe the mode of binding of heregulin to ErbB3. The data suggest instead "partial bivalency" in which each interface is only contributing partially to the joined binding pocket.

Using the crystal structure of EGFR with bound ligand as a model, it is not clear what additional factors would diminish the ability of each interface to fully contribute to the interactions with the ligand. However, no structure of ErbB3 with bound ligand is available to date, and while the same overall structural framework is expected for this complex, our data suggest significant differences in details of the interaction of both receptors with their respective ligands, specifically with respect to contributions made by domain I. A similar shift in the relative contribution to binding from domain III, as seen for EGFR, to domain I has also been reported for the ErbB4 receptor (*48*). It is also important to keep in mind that it is not clear what binding mode the existing EGFR dimer structure represents. Both EGFR and ErbB3 have a high and low affinity mode of binding, and the structural cause for these differences is not clear at this point. The binding constants reported here for ErbB3 and in most other sources reflect the binding of ligand to ErbB3 alone. ErbB3 differs from EGFR in that ligand binding is compatible with spontaneously formed dimers, but the ECD dimers are not stabilized by the presence of ligand (*34*, *35*). Although the low nanomolar binding is tight compared to the binding observed for the ECD of EGFR, it does in fact represent the "low" affinity binding mode for ErbB3. In a cellular setting, ErbB3/ErbB2 heterodimers constitute the high affinity receptor for heregulin β (*39*). This difference can be recapitulated with ECDs that are artificially held together by IgG fusion proteins (*40*) which generate high affinity binding for ErbB3/ErbB2 heterodimeric ECDs (0.013 nM) but not for ErbB3 homodimers (9 nM).

Some additional insight into the question of the relative contributions of the different interfaces in the full-length ErbB3 receptor is provided by the previous limited proteolysis study on ErbB3-ECD (*27*). In this study, limited proteolysis resulted in two cleavage events, one in domain I and one in domain II. While the cleavage in domain II was inconsequential to ligand binding and resulted in disulfide bridged fragments, the cleavage near position 31 of domain I (formerly numbered as residue 50) abolished almost all ligand binding and inversely could be blocked by the binding of ligand. Combined with the data presented here, this would argue that domain III in isolation retains strong binding to ligand, possibly reflecting a binding scheme that is conserved between EGFR and ErbB3, but that the loss of full bivalency in the context of the full-length ErbB3 receptor is mainly the consequence of a loss of the contributions provided by domain III. However, a more detailed insight into this question will have to await the crystal structure of ErbB3-ECD with bound ligand.

Both Locked and Wild-Type ECD Retain Binding at Endosome pH. We surprisingly found that not only was the ability of the locked form to bind ligand retained at low pH but its affinity for heregulin was enhanced. A similar increase in affinity was observed for the ECD^{I-II} construct by SPR measurements, and the enhanced ability of ECD^{I-II} to bind heregulin at low pH was qualitatively confirmed in pull-down studies at low ligand concentrations. This gain in affinity for the ECD^{I-II} construct suggests that its contribution compensates for the loss of binding observed in domain III, thus giving the entire ECD the ability to retain binding at low pH. This observation is consistent with our previous finding that ErbB3 is distinct from EGFR in that its domain I has a more prominent role in binding. Likewise, the pronounced difference in pH dependency of ligand binding between EGFR and ErbB3 can be directly accounted for by the pH dependent interaction of domain I in ErbB3.

The distinct ability of ErbB3 to retain ligand at endosome pH may be of relevance in the context of ligand recycling and the divergent routing of different ErbB members following endocytosis. Endocytosed ErbB receptors travel to early endosomes from which they can either proceed to degradation via late endosomes or return to the cell surface via recycling endosomes. These stages of endocytosis are marked by various degrees of acidification of the vesicles. Early and sorting endosomes have a pH around 6.0; late endosomes continue to be acidified and may reach pH values as low as 5.0. In the case of the heregulin-activated heterodimers of ErbB2 and ErbB3, both receptors preferentially follow different routes. As is the case for EGF-activated EGFR, ErbB2 is mainly targeted for degradation while ErbB3 is to a larger extent recycled (*49*, *50*). It is therefore intriguing that wild-type ErbB3 in contrast to EGFR retains ligand binding at endosome pH and the locked conformation even shows a strong pH minimum at pH 5.5.

The Formation of the Lock Is Suppressed on the Cell Surface. While our binding data demonstrate that ErbB3-ECD in the locked conformation retains strong ligand binding, the question remains about the relative abundance of the locked conformation and hence the contribution of this conformation to signaling. The mutations required for the expression of a stably disulfide locked ECD reside in positions of the dimerization loop of ErbB3 which are known from work on EGFR to destroy ligand-induced activation. Hence the fact that ECD^{L} based chimera show constitutive phosphorylation but fail to respond to heregulin is not informative with respect to the role of the locked conformation in signaling. However, we were able to confirm that ECD^{L} based chimera express well, do not form intermolecular disulfide bridges, and do in fact show elevated constitutive phosphorylation, as was reported for the corresponding domain II mutants of EGFR (*13*, *21*). Moreover, a significant portion of the ECD^{L} based chimera had free cysteines that could be derivatized on the cell surface with iodoacetyl biotin. Soluble ECD^{L} forms the disulfide-stabilized lock quantitatively and has to be processed by the same secretion machinery. The data on cellular ECD^{L} would

therefore suggest that at least a significant portion of the receptors that are anchored to the cell surface are held in a conformation that prevents the formation of the lock and is also sufficiently restraining to prevent spontaneous formation of disulfide bridges between receptors.

We have previously reported an enhanced tendency of the ECD of ErbB3 to form oligomers (*41*) which are formed from ECDs in the extended conformation (*34*). Such oligomerization would be enhanced on the cell surface, and would be one possible mechanism by which receptors are kept in an extended conformation. Molecular models of oligomers show that this would not place the engineered cysteines in a suitable position for intramolecular disulfide bridge formation (data not shown). Mutations in domain IV disable the lock but have no significant impact on the activation of either EGFR or ErbB3−ErbB2 chimera. Hence, our observation of a large portion of nonlocked ECD^L chimera on the cell surface is consistent with the assumption that the locked conformation plays a minor role in this cellular compartment. However, the fact that both wild-type ECD and especially ECD^L show strong binding at endosome conditions opens the possibility in the case of ErbB3 that the locked conformation may play a more important role in this compartment than is evident from binding data and initial activation responses of cell surface localized receptors. However, a direct evaluation of the role of the locked conformation in the endosome compartment will require different experimental approaches.

In conclusion, we have generated a constitutively locked version of the ECD of ErbB3 by introducing a disulfide bridge into the tether region between domains II and IV of ErbB3, and confirmed the formation of the additional disulfide bridge in the secreted ECD. The constitutively locked ECD^L shows strong binding to ligand, indicating that it cannot be discounted as a biologically relevant species, solely on the basis of having a disrupted ligand binding pocket. Although structurally incompatible with models for ligand-induced activation, it can participate in ligand capturing and retention thereby facilitating the transition into the higher affinity mode, found in the extended conformation, which harvests some but not all of the contributions of both binding interfaces to binding. Interestingly, the locked form retains binding at endosome pH, a feature that it shares with wild-type ECD. This binding behavior is in contrast to the ECD of EGFR which loses affinity at low pH. The reported binding properties of EGFR are more closely matched by a truncated construct of the ErbB3-ECD containing only domains III and IV which also loses most of its ability to bind ligand at pH 5.5. The stronger contribution of domain I of ErbB3 to ligand binding, compared to EGFR, is therefore matched by the ability of this domain to use its enhanced binding at low pH to compensate for the loss of binding by domain III, thus maintaining an overall high affinity of ErbB3 to ligand at endosome pH. Initial results obtained for a cellular version of ECD^L suggest that the lock does not engage on the cell surface, at least for a large portion of the receptors. The relatively strong binding of ligand by the constitutively locked form of ErbB3 at endosome pH suggests that this conformation could potentially play a more important role in endosomes than it appears to have on the cell surface.

NOTE ADDED IN PROOF

A recent structure of the ECD of ErbB4 reveals another example of a locked or tethered conformation (*58*). This study also compared the pH dependency of ligand binding to wild-type ErbB1, ErbB3, and ErbB4. The ECDs of ErbB3 and ErbB4 retained ligand binding at low pH. In contrast, the ECD of ErbB1 lost its affinity for EGF and TGF-α at pH 5.5 but retained binding to betacellulin.

ACKNOWLEDGMENT

The acquisition of CD spectra and SPR measurements and analytical ultracentrifugation were carried out in the DOE instrumentation facility at UCLA. We thank Dr. Salem Faham for his help in the structure-based design of disulfide mutants. We thank Dr. Joseph Loo and Cathy Kaddis with help on MALDI-TOF analysis and Dr. Martin Phillips for carrying out the analytical ultracentifugation.

REFERENCES

1. Rubin, I., and Yarden, Y. (2001) The basic biology of HER2, *Ann. Oncol. 12* (Suppl. 1), S3−8.
2. Guy, P. M., Platko, J. V., Cantley, L. C., Cerione, R. A., and Carraway, K. L. r. (1994) Insect cell-expressed p180erbB3 possesses an impaired tyrosine kinase activity, *Proc. Natl. Acad. Sci. U.S.A. 91*, 8132−6.
3. Tzahar, E., Pinkas-Kramarski, R., Moyer, J. D., Klapper, L. N., Alroy, I., Levkowitz, G., Shelly, M., Henis, S., Eisenstein, M., Ratzkin, B. J., Sela, M., Andrews, G. C., and Yarden, Y. (1997) Bivalence of EGF-like ligands drives the ErbB signaling network, *EMBO J. 16*, 4938−50.
4. Dougall, W. C., Qian, X., and Greene, M. I. (1993) Interaction of the neu/p185 and EGF receptor tyrosine kinases: implications for cellular transformation and tumor therapy, *J. Cell. Biochem. 53*, 61−73.
5. Berchuck, A., Kamel, A., Whitaker, R., Kerns, B., Olt, G., Kinney, R., Soper, J. T., Dodge, R., Clarke-Pearson, D. L., Marks, P., et al. (1990) Overexpression of HER-2/neu is associated with poor survival in advanced epithelial ovarian cancer, *Cancer Res. 50*, 4087−91.
6. Schneider, P. M., Hung, M. C., Chiocca, S. M., Manning, J., Zhao, X. Y., Fang, K., and Roth, J. A. (1989) Differential expression of the c-erbB-2 gene in human small cell and non-small cell lung cancer, *Cancer Res. 49*, 4968−71.
7. Yokota, J., Yamamoto, T., Miyajima, N., Toyoshima, K., Nomura, N., Sakamoto, H., Yoshida, T., Terada, M., and Sugimura, T. (1988) Genetic alterations of the c-erbB-2 oncogene occur frequently in tubular adenocarcinoma of the stomach and are often accompanied by amplification of the v-erbA homologue, *Oncogene 2*, 283−7.
8. Slamon, D. J., Godolphin, W., Jones, L. A., Holt, J. A., Wong, S. G., Keith, D. E., Levin, W. J., Stuart, S. G., Udove, J., Ullrich, A., and Press, M. (1989) Studies of the HER-2/neu proto-oncogene in human breast and ovarian cancer, *Science 244*, 707−12.
9. Chantry, A. (1995) The kinase domain and membrane localization determine intracellular interactions between epidermal growth factor receptors, *J. Biol. Chem. 270*, 3068−73.
10. Sherrill, J. M., and Kyte, J. (1996) Activation of epidermal growth factor receptor by epidermal growth factor, *Biochemistry 35*, 5705−18.
11. Moriki, T., Maruyama, H., and Maruyama, I. N. (2001) Activation of preformed EGF receptor dimers by ligand-induced rotation of the transmembrane domain, *J. Mol. Biol. 311*, 1011−26.
12. Yu, X., Sharma, K. D., Takahashi, T., Iwamoto, R., and Mekada, E. (2002) Ligand-independent dimer formation of epidermal growth factor receptor (EGFR) is a step separable from ligand-induced EGFR signaling, *Mol. Biol. Cell 13*, 2547−57.
13. Walker, F., Orchard, S. G., Jorissen, R. N., Hall, N. E., Zhang, H.-H., Hoyne, P. A., Adams, T. E., Johns, T. G., Ward, C., Garrett, T. P. J., Zhu, H.-J., Nerrie, M., Scott, A. M., Nice, E. C., and Burgess, A. W. (2004) CR1/CR2 Interactions Modulate the Functions of the Cell Surface Epidermal Growth Factor Receptor, *J. Biol. Chem. 279*, 22387−98.

14. Gotoh, N., Tojo, A., Hino, M., Yazaki, Y., and Shibuya, M. (1992) A highly conserved tyrosine residue at codon 845 within the kinase domain is not required for the transforming activity of human epidermal growth factor receptor, *Biochem. Biophys. Res. Commun. 186*, 768−74.
15. Stamos, J., Sliwkowski, M. X., and Eigenbrot, C. (2002) Structure of the epidermal growth factor receptor kinase domain alone and in complex with a 4-anilinoquinazoline inhibitor, *J. Biol. Chem. 277*, 46265−72.
16. Cohen, S., and Fava, R. A. (1985) Internalization of functional epidermal growth factor:receptor/kinase complexes in A-431 cells, *J. Biol. Chem. 260*, 12351−8.
17. Kay, D. G., Lai, W. H., Uchihashi, M., Khan, M. N., Posner, B. I., and Bergeron, J. J. (1986) Epidermal growth factor receptor kinase translocation and activation in vivo, *J. Biol. Chem. 261*, 8473−80.
18. Wang, Y., Pennock, S., Chen, X., and Wang, Z. (2002) Endosomal signaling of epidermal growth factor receptor stimulates signal transduction pathways leading to cell survival, *Mol. Cell. Biol. 22*, 7279−90.
19. Garrett, T. P., McKern, N. M., Lou, M., Elleman, T. C., Adams, T. E., Lovrecz, G. O., Zhu, H. J., Walker, F., Frenkel, M. J., Hoyne, P. A., Jorissen, R. N., Nice, E. C., Burgess, A. W., and Ward, C. W. (2002) Crystal structure of a truncated epidermal growth factor receptor extracellular domain bound to transforming growth factor alpha, *Cell 110*, 763−73.
20. Ogiso, H., Ishitani, R., Nureki, O., Fukai, S., Yamanaka, M., Kim, J. H., Saito, K., Sakamoto, A., Inoue, M., Shirouzu, M., and Yokoyama, S. (2002) Crystal structure of the complex of human epidermal growth factor and receptor extracellular domains, *Cell 110*, 775−87.
21. Mattoon, D., Klein, P., Lemmon, M. A., Lax, I., and Schlessinger, J. (2004) The tethered configuration of the EGF receptor extracellular domain exerts only a limited control of receptor function, *Proc. Natl. Acad. Sci. U.S.A. 101*, 923−8.
22. Garrett, T. P., McKern, N. M., Lou, M., Elleman, T. C., Adams, T. E., Lovrecz, G. O., Kofler, M., Jorissen, R. N., Nice, E. C., Burgess, A. W., and Ward, C. W. (2003) The crystal structure of a truncated ErbB2 ectodomain reveals an active conformation, poised to interact with other ErbB receptors, *Mol. Cell 11*, 495−505.
23. Cho, H. S., Mason, K., Ramyar, K. X., Stanley, A. M., Gabelli, S. B., Denney, D. W., and Leahy, D. J. (2003) Structure of the extracellular region of HER2 alone and in complex with the Herceptin Fab, *Nature 412*, 756−60.
24. Sliwkowski, M. X. (2003) Ready to partner, *Nat. Struct. Biol. 10*, 158−9.
25. Cho, H. S., and Leahy, D. J. (2002) Structure of the extracellular region of HER3 reveals an interdomain tether, *Science 297*, 1330−3.
26. Ferguson, K. M., Berger, M. B., Mendrola, J. M., Cho, H. S., Leahy, D. J., and Lemmon, M. A. (2003) EGF activates its receptor by removing interactions that autoinhibit ectodomain dimerization, *Mol. Cell 11*, 507−17.
27. Singer, E. M., Landgraf, R., Horan, T., Slamon, D. J., and Eisenberg, D. (2001) Identification of a Heregulin Binding Site in HER3 Extracellular Domain, *J. Biol. Chem. 276*, 44266−74.
28. Wu, D. G., Wang, L. H., Chi, Y., Sato, G. H., and Sato, J. D. (1990) Human epidermal growth factor receptor residue covalently cross-linked to epidermal growth factor, *Proc. Natl. Acad. Sci. U.S.A. 87*, 3151−5.
29. Woltjer, R. L., Lukas, T. J., and Staros, J. V. (1992) Direct identification of residues of the epidermal growth factor receptor in close proximity to the amino terminus of bound epidermal growth factor, *Proc. Natl. Acad. Sci. U.S.A. 89*, 7801−5.
30. Kohda, D., Odaka, M., Lax, I., Kawasaki, H., Suzuki, K., Ullrich, A., Schlessinger, J., and Inagaki, F. (1993) A 40-kDa epidermal growth factor/transforming growth factor alpha- binding domain produced by limited proteolysis of the extracellular domain of the epidermal growth factor receptor, *J. Biol. Chem. 268*, 1976−81.
31. Lemmon, M. A., Bu, Z., Ladbury, J. E., Zhou, M., Pinchasi, D., Lax, I., Engelman, D. M., and Schlessinger, J. (1997) Two EGF molecules contribute additively to stabilization of the EGFR dimer, *EMBO J. 16*, 281−94.
32. Burgess, A. W., Cho, H. S., Eigenbrot, C., Ferguson, K. M., Garrett, T. P., Leahy, D. J., Lemmon, M. A., Sliwkowski, M. X., Ward, C. W., and Yokoyama, S. (2003) An open-and-shut case? Recent insights into the activation of EGF/ErbB receptors, *Mol. Cell 12*, 541−52.
33. Schlessinger, J. (2002) Ligand-induced, receptor-mediated dimerization and activation of EGF receptor, *Cell 110*, 669−72.
34. Kani, K., Warren, C. M., Kaddis, C. S., Loo, J. A., and Landgraf, R. (2005) Oligomers of ERBB3 have two distinct interfaces that differ in their sensitivity to disruption by heregulin, *J. Biol. Chem. 280*, 8238−47.
35. Berger, M. B., Mendrola, J. M., and Lemmon, M. A. (2004) ErbB3/HER3 does not homodimerize upon neuregulin binding at the cell surface, *FEBS Lett. 569*, 332−6.
36. Fleishman, S. J., Schlessinger, J., and Ben-Tal, N. (2002) A putative molecular-activation switch in the transmembrane domain of erbB2, *Proc. Natl. Acad. Sci. U.S.A. 99*, 15937−40.
37. Mendrola, J. M., Berger, M. B., King, M. C., and Lemmon, M. A. (2002) The single transmembrane domains of ErbB receptors self-associate in cell membranes, *J. Biol. Chem. 277*, 4704−12.
38. Holmes, W. E., Sliwkowski, M. X., Akita, R. W., Henzel, W. J., Lee, J., Park, J. W., Yansura, D., Abadi, N., Raab, H., Lewis, G. D., Shepard, H. M., Kuang, W. J., Wood, W. I., Goeddel, D. V., and Vandlen, R. L. (1992) Identification of heregulin, a specific activator of p185erbB2, *Science 256*, 1205−10.
39. Sliwkowski, M. X., Schaefer, G., Akita, R. W., Lofgren, J. A., Fitzpatrick, V. D., Nuijens, A., Fendly, B. M., Cerione, R. A., Vandlen, R. L., and Carraway, K. L. r. d. (1994) Coexpression of erbB2 and erbB3 proteins reconstitutes a high affinity receptor for heregulin, *J. Biol. Chem. 269*, 14661−5.
40. Fitzpatrick, V. D., Pisacane, P. I., Vandlen, R. L., and Sliwkowski, M. X. (1998) Formation of a high affinity heregulin binding site using the soluble extracellular domains of ErbB2 with ErbB3 or ErbB4, *FEBS Lett. 431*, 102−6.
41. Landgraf, R., and Eisenberg, D. (2000) Heregulin reverses the oligomerization of HER3, *Biochemistry 39*, 8503−11.
42. Cohn, E. J., and Edsall, J. T. (1943) Density and apparent specific volume of proteins, in *Proteins, Amino Acids and Peptides as Ions and Dipolar Ions*, Reinhold Publishing Corporation, New York.
43. Laue, T. M., Shah, B. D., Ridgeway, T. M., and Pelletier, S. L. (1992) Computer Aided Interpretation of Analytical Sedimentation Data for Proteins, in *Analytical Ultracentrifugation in Biochemistry and Polymer Science*, The Royal Society of Chemistry, Cambridge, U.K.
44. Durschschlag, H. (1986) *Specific Volumes of Biological Macromolecules and Some Other Molecules of Biological Interest*, Springer-Verlag, Berlin.
45. Era, T., Wong, S., and Witte, O. N. (2002) Analysis of Bcr-Abl function using an in vitro embryonic stem cell differentiation system, *Methods Mol. Biol. 185*, 83−95.
46. Petersen, M. T., Jonson, P. H., and Petersen, S. B. (1999) Amino acid neighbours and detailed conformational analysis of cysteines in proteins, *Protein Eng. 12*, 535−48.
47. Jones, T. A., Zou, J. Y., Cowan, S. W., and Kjeldgaard. (1991) Improved methods for building protein models in electron density maps and the location of errors in these models, *Acta Crystallogr. A 47* (Part 2), 110−9.
48. Kim, J. H., Saito, K., and Yokoyama, S. (2002) Chimeric receptor analyses of the interactions of the ectodomains of ErbB-1 with epidermal growth factor and of those of ErbB-4 with neuregulin, *Eur. J. Biochem. 269*, 2323−9.
49. Waterman, H., Sabanai, I., Geiger, B., and Yarden, Y. (1998) Alternative intracellular routing of ErbB receptors may determine signaling potency, *J. Biol. Chem. 273*, 13819−27.
50. Waterman, H., and Yarden, Y. (2001) Molecular mechanisms underlying endocytosis and sorting of ErbB receptor tyrosine kinases, *FEBS Lett. 490*, 142−52.
51. Jones, J. T., Akita, R. W., and Sliwkowski, M. X. (1999) Binding specificities and affinities of egf domains for ErbB receptors, *FEBS Lett. 447*, 227−31.
52. Jones, J. T., Ballinger, M. D., Pisacane, P. I., Lofgren, J. A., Fitzpatrick, V. D., Fairbrother, W. J., Wells, J. A., and Sliwkowski, M. X. (1998) Binding interaction of the heregulinbeta egf domain with ErbB3 and ErbB4 receptors assessed by alanine scanning mutagenesis, *J. Biol. Chem. 273*, 11667−74.
53. Lee, H., Akita, R. W., Sliwkowski, M. X., and Maihle, N. J. (2001) A naturally occurring secreted human ErbB3 receptor isoform inhibits heregulin-stimulated activation of ErbB2, ErbB3, and ErbB4, *Cancer Res. 61*, 4467−73.

54. Horan, T., Wen, J., Arakawa, T., Liu, N., Brankow, D., Hu, S., Ratzkin, B., and Philo, J. S. (1995) Binding of Neu differentiation factor with the extracellular domain of Her2 and Her3, *J. Biol. Chem. 270*, 24604−8.

55. Carraway, K. L. r., Sliwkowski, M. X., Akita, R., Platko, J. V., Guy, P. M., Nuijens, A., Diamonti, A. J., Vandlen, R. L., Cantley, L. C., and Cerione, R. A. (1994) The erbB3 gene product is a receptor for heregulin, *J. Biol. Chem. 269*, 14303−6.

56. Tzahar, E., Levkowitz, G., Karunagaran, D., Yi, L., Peles, E., Lavi, S., Chang, D., Liu, N., Yayon, A., Wen, D. Z., and Yarden, Y. (1994) ErbB-3 and ErbB-4 function as the respective low and high affinity receptors of all Neu differentiation factor/heregulin isoforms, *J. Biol. Chem. 269*, 25226−33.

57. Ferguson, K. M., Darling, P. J., Mohan, M. J., Macatee, T. L., and Lemmon, M. A. (2000) Extracellular domains drive homo- but not hetero-dimerization of erbB receptors, *Embo. J. 19*, 4632−43.

58. Bouyain, S., Longo, P. A., Li, S., Ferguson, K. M., and Leahy, D. J. (2005) The extracellular region of ErbB4 adopts a tethered conformation in the absence of ligand, *Proc. Natl. Acad. Sci. U.S.A. 102*, 15024−9.

BI0515220